Universitat Politècnica de Catalunya (UPC)
Universitat Autònoma de Barcelona (UAB)
Universitat de Barcelona (UB)
Institut de Ciències Fotòniques (ICFO)

http://www.photonicsbcn.eu

Master in Photonics

MASTER THESIS WORK

Generation of artificial thermal sources and their characterization by intensity interferometry

Alejandro Martínez Jiménez

Supervised by Prof. Enrique Josua Fernández (UM)
Co-supervised by Prof. Jordi Mompart Penina (UAB)

Presented on date 9th September 2020

Registered at

Escola Tècnica Superior d'Enginyeria de Telecomunicació de Barcelona

Generation of artificial thermal sources and their characterization by intensity interferometry

Alejandro Martínez Jiménez[1]

[1]Laboratorio de Óptica, Centro de Investigación en Óptica y Nanofísica (CiOyN), Universidad de Murcia, Campus de Espinardo (Ed. 34), 30010 Murcia

E-mail: alejandromarjim@gmail.com

September 1^{st}, 2020

Abstract. The Hanbury Brown and Twiss (HB-T) effect is fundamental to understand the nature of light, with important applications, for instance in ghost imaging. In this work, some coherence properties of the light emitted by an artificial source were investigated. In particular, the second-order coherence function in time was retrieved under different experimental conditions. The work included the generation of pseudothermal light by using distinct rotating diffusers. The emitters were then characterized by setting an intensity interferometer (also called Hanbury Brown-Twiss interferometer). This procedure allowed to measure the photon bunching, or equivalently whether and how photons were eventually grouped at the detector. The results showed that the variation of the rotation speed of the diffuser played a role in the second-order temporal coherence function, particularly when low rotation speeds were considered.

Keywords: Hanbury Brown and Twiss effect, photon bunching, optical coherence, intensity interferometry, pseudothermal light

1. Introduction

The term *"photon bunching"* is used within the context of intensity interferometry, HB-T effect. A sketch of the HB-T interferometer is shown in Fig.1. Detectors $D1$ and $D2$ are at the same distance from the beam splitter for classical second-order temporal coherence function. This experimental setup measures a delayed coincidence rate where one of the detectors registers a count at time t and the other a count at $t+\tau$. If τ, the time delay, is smaller than the coherence time τ_0, information on the statistics of the light beam striking the beam splitter can be determined.

Mathematically, bunching appears when $g^{(2)}(0) > g^{(2)}(\tau)(\tau \neq 0)$, being $g^{(2)}(\tau)$ the normalized second-order coherence function, and τ the time difference between photon detection events. If the average of the intensity at each detector is $\langle I_1(t)\rangle$ and $\langle I_2(t)\rangle$ then, the probability of obtaining a coincidence count with a time delay τ is:

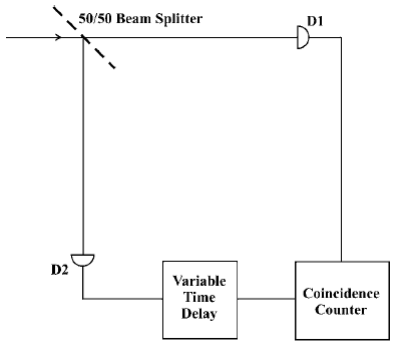

Figure 1: Sketch of the setup for the Hanbury-Brown and Twiss interferometer. Source [1]

$$g^{(2)}(\tau) = \frac{\langle I_1(t) I_2(t-\tau)\rangle}{\langle I_1(t)\rangle \langle I_2(t)\rangle} \tag{1}$$

This is the classical second-order temporal coherence function. If the detectors are at different distances from the beam splitter, we would speak about second-order spatial coherence function. Photon bunching essentially describes how photons are grouped at the detector. It is a property of thermal emitters, which statistically procedure photons in packs of 2 units. When the bunching effect was discovered [2], some authors tried to measure it, but not all of them found bunching in the laboratory. This fact created great controversy [3]; basically in two debates. Brannen and Fergusen (1956) [4] discussed whether light correlation existed or not, if so, it should be made *"A major revision of some fundamental concepts in quantum mechanics"*. The debate ended accepting the reality of photon bunching. Once accepted, the findings of Hanbury Brown and Twiss were of great importance in Physics. It was the cornerstone for the development of optical coherence theory and quantum optics [5].

At the beginning of the development of photon bunching theory, it was assumed that only photons via spontaneous parametric down conversion (SPDC) could be correlated [6]. Both, classical and quantum theories can predict the bunching effect, although some authors still suggest the need of a new frame [7]. In recent years, there has been growing interest in ghost imaging and intensity interferometry [8], due to improving the efficiency of nonlinear microscopy processes like second harmonic generation (SHG) and two photon excited flourescence (TPEF) [9]. Furthermore, theory predicts a linear proportionality between second-order coherence and two photon absorption (TPA) [10]. More recently, there has been increasing interest in superbunching [7, 11–14]. The term superbunching is employed when $g^{(2)}(0)$ is larger than 2. Quantum theory could predict it [13], relating bunching withs different yet indistinguishable photon paths, that reaching the detector. Adding indistinguishable paths can this way generate increased bunching for photons.

An interesting topic is how different experimental parameters can affect the bunching effect. In this research, we generated an artificial thermal source with a laser and some rotating diffusers. We characterized how the variation of different parameters influenced the measured bunching. The light intensity distribution plays an important role. The Poissonian distribution of the photons emitted by laser changes when light is enforced to pass through the rotating diffuser, turning into a negative exponential distribution. It can be demonstrated that the qth momentum of intensity in negative exponential distribution P_I, is:

$$\langle I^q \rangle = \int_0^\infty I^q P_I(I) dI = \langle I \rangle^q (q!)^2 \tag{2}$$

Taking into account the normalized second-order coherence function, for one rotating glass $g^{(2)}(0) = 2$. Several studies [11,13] calculated the second-order coherence function, obtaining Eq.3.

$$g^{(2)}(\tau) = 1 + \mathrm{sinc}^2\left(\frac{\Delta\omega \cdot \tau}{2}\right) \tag{3}$$

Being $\Delta\omega$ the spectral bandwidth of the source through the diffuser, and τ the time between light detection. This equation will be taken in the following to describe the experimental data.

2. Methods

The light intensity correlations can be obtained by measuring the second-order coherence function. Characterization of photon bunching [7,11] typically employs interferometry, or also called Hanbury Brown and Twiss experiment, to measure light correlations. A basic HB-T setup consists of a beam splitter, two detectors separated spacially the same distance, and a coincidence counter. The limitation of this approach is that the alignment could be complicated. In recent years, the standard setup has been changed to use a fiber beam splitter [13]. In our study, APD has been used as light detector.

2.1. Experimental system

The experimental setup to generate and characterize photon bunching is shown in Fig.2. The employed laser is a single-mode continuous wave laser with central wavelength at $670nm$ (Thorlabs, CPS670F) with maximum power of $4.5mW$. The rotating ground glass holder (RGGH) is a rotating holder required to mount the set of diffusers, manufactured specifically for this experiment. ML is an objective microscope lens with 5x magnification, 0.10 numerical aperture and $25.4mm$ of focal length (Newport, M-5X). DK is the diffusers kit, with N-BK7 substrate (Thorlabs, DGK01) and two engineered circle diffusers (Thorlabs, ED1-C20, ED1-C50). These diffusers consist on

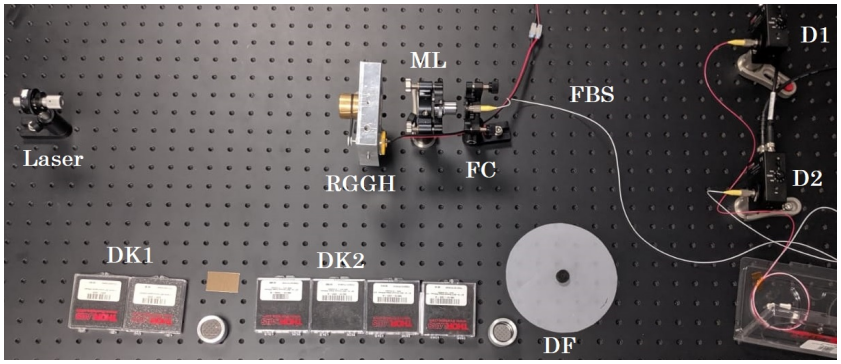

Figure 2: Experimental setup for generating a pseudothermal light source with one diffuser. Laser: single-mode continuous-wave laser. DK: Diffusers kits, grit and holography. RGGH: Rotating ground glass holder (see section in appendix A1). ML: Microscope objective lens. FC: Fiber coupler FBS: nonpolarized 50:50 fiber beam splitter. D: Silicon Avalanche photodetector. DF: Diffuser film.

uniform surface patterns across the entire clear aperture. FBS is a monomode fiber optic coupler, 50:50 and a numerical aperture of 0.13 (Thorlabs, TN670R5F1). The diameter of FBS is $3.5\mu m$. The fiber coupler has a FC connector. D_1 and D_2 are two Silicon avalanche photodetectors (Thorlabs, APD410A/M). The maximum responsivity ($\mathfrak{R}_M(\lambda)$ to estimate the output voltage) is at $800nm$.

$$V_{out} = P_{opt} \times \mathfrak{R}_M(\lambda) \times G \tag{4}$$

The amplifier's transimpedance gain G is $500kV/A$. The maximum output voltage swing of output is $2.0V$ into 50Ω. The optical damage threshold input power is $1mW$. The output voltage frequency of the APD is $10MHz$. To avoid damage on the APD, a neutral density filter has been used, not shown in Fig.2 (Thorlabs, NDC-50C).
Seven different rotating ground glass diffusers have been used, the diffuser film is connected to 3V-DC motor Fig.4(a) with a ten stage dimmer. Professional diffusers with 120, 220, 600 and 1500 grit polishes. The various grits provide a range from fine to coarse scattering. A finer grit (e.g., 1500) allows higher transmission, while a coarser grit (e.g., 120) creates a wider diffusion pattern at the expense of transmission. Others engineered diffusers with a holography pattern have been used with different angles. All professional diffusers have been connected to an additional motor 9V supplied with a dimmer, and also to variable 50V-3A DC power supply (Nafcom, HY5003). In summary, the diffuser film has a 3V-DC motor, and all the rest of the diffusers have a 9V-DC motor 4(b). However, the 9V-DC motor is not valid for analysing a wide range of velocities.

The output signal of the detectors is carried for a field-programmable gate array (FPGA)-based (Moku:Lab, Liquid Instruments, Australia). There are many tools provided by the Moku ‡. Data logger shown in Fig.3(b) has allowed us to record large time files. However, there are certain drawbacks associated with the use of Data

‡ Moku:Lab instruments

logger since the maximum velocity to save the data for two-channel at the same time is $500kSa/s$, insufficient for the majority of experimental work. Lock-in amplifier (LIA, Fig.3(c)) with an external demodulation could be a chance, but the signal has a DC-level, which worsened the result. Oscilloscope instrument in Fig.3(a) could read and save until $500MSa/s$ using both channels, faster than the output voltage. The sample rate required for the experiment is limited by Nyquist frequency of the detectors. It was decided that the best instrument for this investigation was the oscilloscope as the save data speed plays an important role. For practical use in the laboratory, the IOs application has been used, connected to the IP of the local network.

2.2. Experimental protocol

To collect the experimental data, the Moku instrument was set up at the oscilloscope mode, configured for linear data acquisition. Each of the Moku's channels was connected to a 50Ω resistor. Depending on the typical frequency of oscillation of the signal, two different procedures were used. The case when the full width half maximum (FWHM) of the spikes of the signal retrieved by the oscilloscope were in the milisecond (ms) scale and the other case, when that laid on the microsecond range (μs).

When the signal spikes were in the μs region, the Moku was set up at oscilloscope mode, with sampling rate equals to $83.3MSa/s$. The decision to use this velocity was two folds: the velocity of the detector doubled the Nyquist frequency; and to have a accurate sampling in the μs scale. Moku:Oscilloscope mode did not allow to record long sequences. The time span at this velocity was $140\mu s$. After setting Moku, data were recorded on MatLab file *.mat*. The analysis of isolated samples provided some deviations from the expected response. Because of that, several bins with the same sample rate and acquisition mode were collected, exactly ten bins for each measurement. All bins were separated in time in an inhomogeneous way. Conversely, in ms regime, data logger setting in the instrument was used. It permitted to record up to 2 minutes at $500kSa/s$. The data collected were recorded on a unique open-source binary file *.li*,

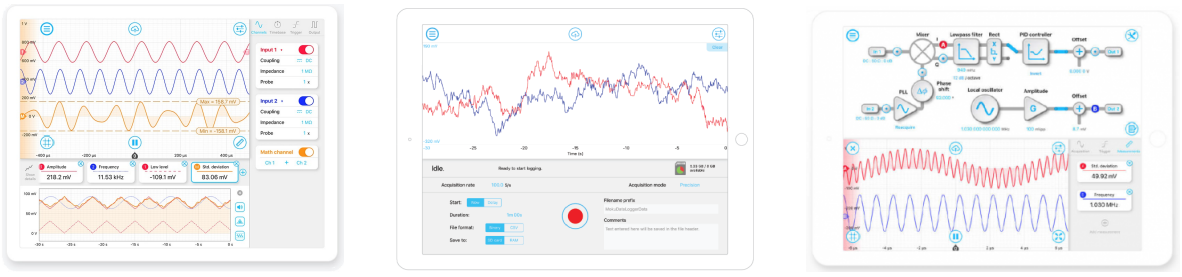

(a) (b) (c)

Figure 3: Screenshot Moku:Lab interface. a) Oscilloscope instrument. Signal in every channel, third channel with a function of A and B channels. b) Data Logger instrument. Configuration setup to record the data. Different acquistion modes, linear, sinc and gaussian. c) Lock-In instrument interface

allowing to register data at maximum velocity. Data converted to *.mat* files were performed using LI file converter. For data processing wide sense ergodicity was assumed. In brief and simplifying the concept: a sufficient large number of small samples in time are equivalent to a single long sample from the statistical point of view. This assumption is widely accepted in the context of optical coherence and statistical optics, so the mathematical treatment of the theoretical frame is significantly simple.

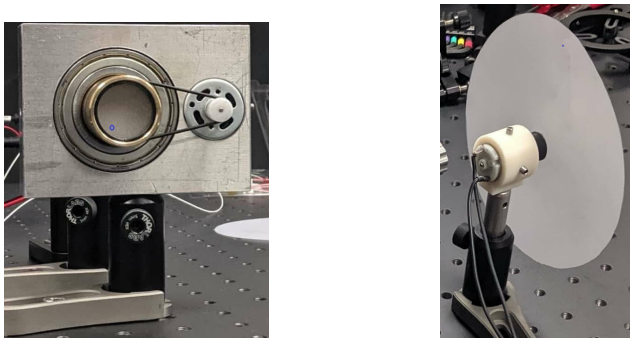

(a) (b)

Figure 4: Angular velocity retrieval method. a) Lab designed rotating holder. A piece of 1 inch diameter was placed on it completely covering the aperture. The paper had a hole through which the beam is focused. b) Diffuser film with a hole.

Once the samples were extracted, in μs bins, a low pass filter to smooth the data series was applied. After that, the correlation across signals was obtained following Eq.1. Proper normalization was applied. All data processing was carried out using Matlab.

In order to calibrate the rotation velocity some prior measurements were taken. The RGGH in Fig.4(a) was covered with a piece of opaque paper endowed with a pinhole. Laser beam was focused on the hole and the light passing through was measured in 1 sec long runs. A similar method was applied to the diffuser film in Fig.4(b).

3. Results

The second-order coherence function of the light was measured. For better visualization, the data sampling was reduced across the figures in this work. Fig.5 shows the measured $g^{(2)}(\tau)$. In Fig.5(a) the measured normalized second-order coherence function when the diffuser film was rotating at 40 Hz is plotted in orange color. The error bars are the standard deviation of the ten bins recorded for each point. The measured second-order coherence function when the diffuser was off is shown with blue dots, with the error bars corresponding to the standard deviation. The sinc function was fitted to the experimental data. Fig.5(b) shows the measured second-order coherence function in the absence of diffuser, with the laser beam hitting directly onto the fiber end.

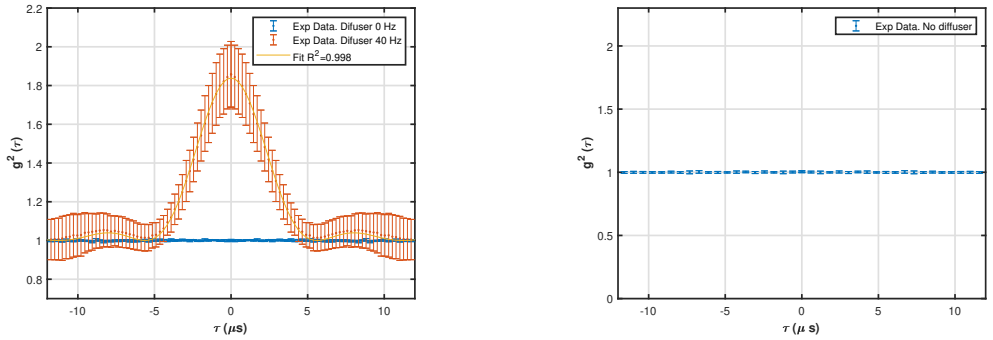

(a) (b)

Figure 5: Measured second-order temporal coherence function $g^{(2)}(\tau)$. $\tau = t_1 - t_2$ is the time difference between two detection events. a) The yellow curve is the sinc function fitting, employing Eq.3. b) Experimental data points of correlations without diffuser. All data were recorded at 83.3 MSa/s

Fig.6 presents the experimental second-order coherence function obtained for different comercial diffusers with distinct grits, rotating at identical speeds. Error bars correspond to the standard deviation in every case. The average correlation peak was $g^{(2)}(0) = 1.80 \pm 0.12$. No significant differences were found when changing the distance to the source in the FWHM ($\tau_{coh} = 4.58 \pm 0.40$) or the peak ($g^{(2)}(0) = 1.86 \pm 0.06$) within the selected range. Additional details and numbers pertaining the results under different distances can be found in the Appendix C1.

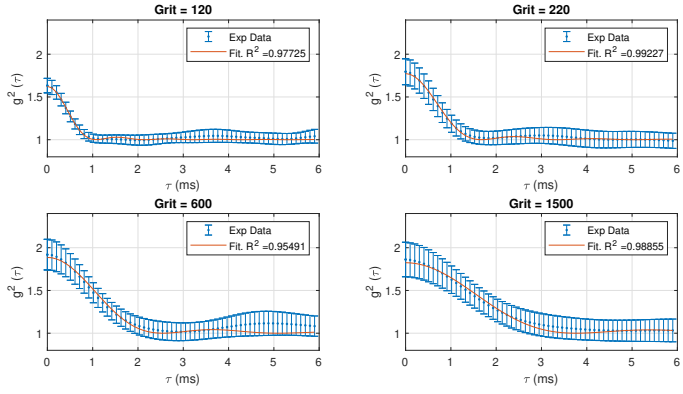

Figure 6: Measured second degree temporal coherence function $g^{(2)}(\tau)$ changing the diffusers in the RGGH. τ is the time difference between detection events within a two-photon coincide counts. In blue color the experimental data points with diffuser at $3Hz$ in blue. The red lines are curve fittings by employing the Eq.3. All data were recorded at $500kSa/s$

Every result from the RGGH in Fig.7 were obtained at distance $102.5mm$ between the diffuser and the FC. We show the experimental data points in blue color, error bars as the standard deviation, and the curve fitting is decipted in red color. Measurements were

taken changing the velocity of rotation of the diffusers. The equivalence between rotation speed and applied voltage were detailed in Appendix C2. There was no significant difference between correlation peak in both setups. From Fig.7, the correlation peak was found at $g^{(2)}(0) = 1.75 \pm 0.16$.

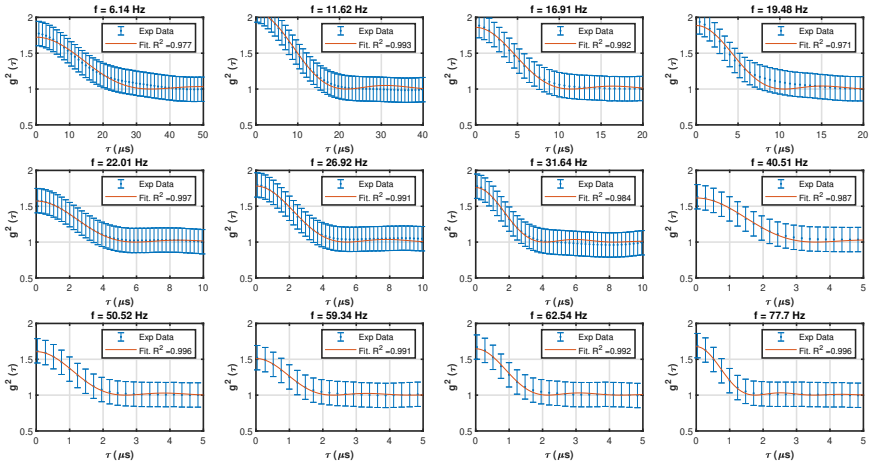

Figure 7: Measured second degree temporal coherence function $g^{(2)}(\tau)$ changing rotation speed in the diffuser film.τ is the time difference between detection. Experimental data points obtained with the diffuser are shown in blue color. The red lines correspond to the curve fittings employing Eq.3. The axis scale has not been maintained along the panels for better visualization. All data were recorded at $83.3MSa/s$

In order to understand the relationship between second order coherence function and the rotation speed, a separate analysis was performed. A linear fitting was done with the sinc argument of the second-order coherence function and the rotation speed. This results are plotted in Fig.8. A squared correlation coefficient ($R^2 = 0.991$) was found in the linear fitting. Additional details of the fitting, including some other statistical parameters, are shown in Appendix B1, B2.

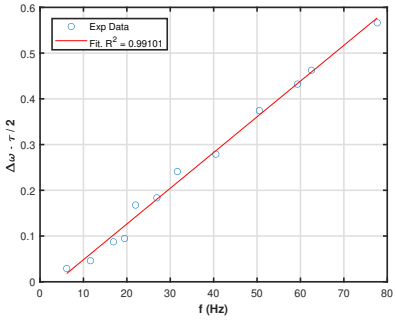

Figure 8: Measured argument of the second-order temporal coherence function $g^{(2)}(\tau)$ changing rotation speed in the diffuser film. Experimental data points in blue color, curve fitting is shown with a red line.

4. Discussion and conclusions

When accomplishing the digital processing of the experimental data, the sample size must be accounted, particularly for long samples. In that situation the average might be overestimated. To ameliorate this effect, the data from small bins were gathered in a single run under the assumption of ergodicity. After that, the processing included the application of a low pass filter $20MHz$ to get rid of high frequency noise. The normalization of the second-order coherence function, also yielded in some cases an subestimation of the curve, detected because of the appearence of negative values. These points are very likely not real in the light beam, in the sense that they would indicate antibunching, which is not expected under the experimental conditions set in the laboratory for this work. Another interesting point to mention here is that Eq.1 could be eventually calculated through the convolution of the signals from each channel in the Fourier space. Nevertheless, we found certain experimental drawbacks associated with the use of a Fourier transform in this particular case. The temporal windows used to calculate the Fourier spectrum might be insufficient, so further windowing and a more refined prefiltering of the signal would be required to operate in the Fourier space. Possibly the procedure could be more efficient once solved the problems to carry on the convolution in the Fourier space, and it is a future line to be explored.

Some results shown in Fig.5(a) might appear counterintuitive when they are confronted to those in Fig.5(b). In particular, we have found that keeping the diffuser with no rotation is, from the point of view of coherence, similar to have the light beam directly out of the laser. This is an important result for imaging, because it establishes that incoherent illumination requires the rotation of the diffuser, not just its implementation in the set up.

Regarding the results presented in Fig.6, a broadening of the sinc argument of the second-order coherence function is found depending on the grit value of the diffusers. When looking at the physical significant of the argument of the sinc function, it could be misunderstood that the spectral bandwidth of the light source was varying during the experiment. That was not the case, because the laser was always emitting in a known range, not compatible with the experimental changes we found. Further theoretical investigation of this fact should be carried out in the future to understand this effect. Our hypothesis so far, yet to be explored, is that the phenomenon might be related with a diffraction grating effect caused by the manufacturing procedure of the diffuser filters.

Another important result from this work is that the rotation speed plays a key role, especially at low speeds, shaping the second-order coherence function. Previous literature about the second-order coherence function with comparable light sources found the time scales in the range of microseconds [7, 11, 12], while in our experiment we measured coherence times in the milisecond range. Further investigation is required to solve the

complete picture.

In summary, this work investigated the impact of different diffusers and rotation speeds on photon bunching through the second-order coherence function. Some interesting results were found, which have been commented above in this section. In the future, photon counters are to be used in place of APDs, so that number of photons can be retrieved rather than fluctuation of light intensity.

Acknowledgements

I must express my sincere appreciation to Dra. Crina Cojocaru for her support in the academic procedures, in the security that without her help this work would not have been possible. Thanks to the workshop staff of Servicios de Apoyo a la Investigación (SAI), mechanical and electrical workshop of the University of Murcia for their contribution. I would like to express my gratitude to my cosupervisor Dr. Jordi Mompart for his important guidance with the theoretical background on the first days. Finally, my special thanks goes to my supervisor Dr. Enrique Josua Fernandez for his continued support, patience and willingness to carry out all the experimental work in the laboratory during the lockdown times caused by the SARS-CoV-2 virus.

References

[1] Gerry C and Knight P 2004 *Introductory Quantum Optics* (Cambridge University Press) ISBN 9780521527354 URL https://www.cambridge.org/core/product/identifier/9780511791239/type/book

[2] Hanbury Brown R and Twiss R Q 1956 *Nature* **178** 1046–1048 ISSN 00280836

[3] Goodman P, Langer W and Brumby S 1997 The Twiss-Hanbury Brown controversy : A 40-years perspective URL https://inis.iaea.org/search/search.aspx?orig_q=RN:29003804

[4] Brannen E and Ferguson H I 1956 *Nature* **178** 481–482 ISSN 00280836

[5] Mandel L and Wolf E 1995 *Optical Coherence and Quantum Optics* (Cambridge University Press) ISBN 9780521417112 URL https://www.cambridge.org/core/product/identifier/9781139644105/type/book

[6] Ou Z Y, Rhee J K and Wang L J 2000 *Frontiers of Laser Physics and Quantum Optics* **60** 331–343

[7] Bai B, Liu J, Zhou Y, Zheng H, Chen H, Zhang S, He Y, Li F and Xu Z 2017 *Journal of the Optical Society of America B* **34** 2081 ISSN 0740-3224

[8] Shirai T 2017 *Modern Aspects of Intensity Interferometry With Classical Light* 1st ed vol 62 (Elsevier B.V.) URL http://dx.doi.org/10.1016/bs.po.2017.01.001

[9] Jechow A, Seefeldt M, Kurzke H, Heuer A and Menzel R 2013 *Nature Photonics* **7** 1–14 URL http://arxiv.org/abs/1310.4297%0Ahttp://dx.doi.org/10.1038/nphoton.2013.271

[10] Mollow B R 1968 *Physical Review* **175** 1555–1563 ISSN 0031899X

[11] Zhou Y, Li F L, Bai B, Chen H, Liu J, Xu Z and Zheng H 2017 *Physical Review A* **95** 1–9 ISSN 24699934

[12] Zhou Y, Luo S, Tang Z, Zheng H, Chen H, Liu J, Li F l and Xu Z 2019 *Journal of the Optical Society of America B* **36** 96 ISSN 0740-3224

[13] Hong P, Liu J and Zhang G 2012 *Physical Review A - Atomic, Molecular, and Optical Physics* **86** 1–4 ISSN 10502947

[14] Zhang L, Zhou D, Lu Y, Zhang H and Zhang G 2020 *Photonics Research* **8** 503 ISSN 2327-9125